JBC Papers in Press. Published on January 19, 2016 as Manuscript M115.711697
The latest version is at http://www.jbc.org/cgi/doi/10.1074/jbc.M115.711697

NF-κB Essential MOdulator (NEMO) Is Critical for Thyroid Function

Carla Reale¶[1], Anna Iervolino¶[1], Ivan Scudiero¶, Angela Ferravante¶, Luca Egildo D' Andrea¶, Pellegrino Mazzone¶, Tiziana Zotti‡, Antonio Leonardi§, Luca Roberto¶, Mariastella Zannini#, Tiziana de Cristofaro#, Muralitharan Shanmugakonarξ, Giovambattista Capasso¶ϕ, Manolis Pasparakis∫, Pasquale Vito¶‡ and Romania Stilo‡§

from

¶ Biogem Consortium, Via Camporeale, 83031 Ariano Irpino, Italy;
‡ Dipartimento di Scienze e Tecnologie, Università del Sannio, Via Port'Arsa 11, 82100 Benevento, Italy;
§ Dipartimento di Medicina Molecolare e Biotecnologie Mediche, Università di Napoli, 80131 Napoli, Italy;
# Istituto di Endocrinologia e Oncologia Sperimentale; CNR, Napoli, Italy;
ϕ Dipartimento di Scienze cardio-toraciche e respiratorie; Seconda Università di Napoli, Italy;
∫ Institute for Genetics, University of Cologne, 50923 Cologne, Germany;
ξ Laboratory Animal Research Centre, Qatar University, PO Box 2713, Doha, Qatar.

Running title: *NEMO is essential for thyroid function*

Address correspondence to P. V. vito@unisannio.it

[1] These authors share the first authorship

Keywords: NF-kappaB (NF-κB), NEMO, thyroid, transgenic mice, gene knockout, thyroid hormone, apoptosis

ABSTRACT

The I-κB kinase (IKK) subunit NEMO/IKKγ (NEMO) is an adapter molecule that is critical for canonical activation of NF-κB, a pleiotropic transcription factor controlling immunity, differentiation, cell growth, tumorigenesis and apoptosis. To explore the functional role of canonical NF-κB signaling in thyroid gland differentiation and function, we have generated a murine strain bearing a genetic deletion of the NEMO locus in thyroid. Here we show that thyrocyte-specific NEMO knockout mice gradually develop hypothyroidism after birth, which leads to reduced body weight and shortened life span. Histological and molecular analysis indicate that absence of NEMO in thyrocytes results in a dramatic loss of the thyroid gland cellularity, associated with down-regulation of thyroid differentiation markers and ongoing apoptosis. Thus, NEMO-dependent signaling is essential for normal thyroid physiology.

INTRODUCTION

The nuclear factor (NF)-κB signaling pathway controls a variety of important biological functions, including immune and inflammatory responses, differentiation, cell growth, tumorigenesis and apoptosis (1). Two distinct pathways of NF-κB activation have been reported. The classical, canonical pathway is found virtually in all mammalian cells and depends on the presence of the IKKγ/NF-κB essential modulator (NEMO) protein (1). In this pathway, NF-κB activation is mediated by the IKK complex, consisting of the IKK1/IKKα and IKK2/IKKβ catalytic kinase subunits and the NEMO regulatory protein (1). Basically, NF-κB transcription factors are kept inactive in the cytoplasm through binding to members of the I-κB family of inhibitory proteins. Cell activation by a variety of stimuli results in the IKK-dependent phosphorylation of I-κB proteins, followed by their polyubiquitination and their proteasome-dependent degradation, allowing NF-κB dimers to enter the nucleus and catalyze transcription of target genes (1). In specific lymphoid tissues cells, an alternative, non-canonical pathway has been described that relies on IKKα-mediated phosphorylation of I-κB molecules. This pathway seems to be independent of NEMO activity (1). Recent publications have

also shown that diverse posttranslational modifications, including ubiquitination, sumoylation and phosphorylation, regulate the function of NEMO in the IKK complex (2-6).

Gene-targeting experiments have shown that mice lacking p65/RelA, IKK2/IKKβ, or NEMO die during embryonic development due to liver apoptosis (7-12). The evidence that NEMO-deficient mice exhibit a phenotype similar to that of p65/RelA-deficient mice demonstrates the essential role of NEMO in the canonical NF-κB signaling. Experiments based on tissue- and/or organ-specific deletion of NEMO, obtained through Cre-mediated genetic recombination, have given diverse results regarding the physiological role of this protein. In fact, ablation of NEMO in liver parenchymal cells causes spontaneous development of steatohepatitis and hepatocellular carcinoma (13). Instead, intestinal epithelial-cell-specific deletion of NEMO results in severe chronic intestinal inflammation due to apoptosis of colonic epithelial cells, impaired expression of antimicrobial peptides and translocation of bacteria into the mucosa (14). Central nervous system-specific ablation of NEMO results in no apparent abnormalities, but rather ameliorates inflammatory and autoimmune pathologies (15). NEMO inactivation in the heart did not affect embryonic cardiac development but led to spontaneous and progressive impairment of cardiac function, progression to dilated cardiomyopathy and heart failure (16). Finally, genetic abrogation of NEMO in podocytes did not affect normal glomerular development and function under non-stressed conditions (17). Thus, it appears that canonical NF-κB signaling performs different roles and functions depending on the type of tissue and organ.

In the present work, we have investigated the requirement for NEMO in thyroid development, differentiation and function by generating a mouse model bearing a thyroid-specific genetic inactivation of NEMO. In these mice, development and differentiation of the thyroid gland appears normal. In contrast, after birth, thyroid-specific NEMO knockout mice develop progressive loss of thyroid cellularity and thyroid markers, hypothyroidism and reduced vitality due to extensive apoptosis of thyroid cells. Thus, our data indicate that NF-κB-dependent gene expression is essential for maintaining normal thyroid gland structure and function in the adult.

EXPERIMENTAL PROCEDURES

Ethics Procedures involving animals were conducted as indicated in the Italian National Guidelines (D.L. No. 100/2006, and D.L. No. 116/1992) and in the pertinent European Directives (EEC Council Directive 86/609, 1.12.1987), adhering to the Guide for the Care and Use of Laboratory Animals (United States National Research Council, 1996). All the in vivo experimental activities were approved by the Animal Ethics Committee (CESA) of Biogem (Italy) with ID no. 4713.

Generation of $NEMO^{TS\text{-}KO}$ mice
To inactivate the NEMO gene in thyroid, mice expressing Cre recombinase under the control of endogenous Pax8 promoter (18) and $NEMO^{Flox/+}$ (12) were bred. $NEMO^{Flox/Y}/Pax8^{Cre/+}$ mice were named $NEMO^{TS\text{-}KO}$ and used as the experimental group, while $NEMO^{+/Y}/Pax8^{Cre/+}$ littermates were used as controls (CTR). Genotyping was performed by PCR analysis of tail biopsy. All experiments were conducted on age and gender-matched animals.

Metabolic measurements
Renal parameters were evaluated in 12-month-old mice using metabolic cages as previously described (19). Mice were housed individually in metabolic cages for 5 days at 23° C with 12 hrs dark/light cycle. After 4 days of adjustment, parameters were registered on day 5. 24 hrs urine output was collected under mineral oil to prevent evaporation. Proteinuria was quantified by Bradford assay, urinary electrolytes and creatinine were evaluated using Vitrovet (Scil).

Histology and Immunohistochemistry
Mice were anesthetized by isoflurane and perfused through abdominal aorta with 4% PFA. Blood, left kidney and thyroid were collected before perfusion. The left kidney and one thyroid lobe were used for immunoblotting or PCR, while the right kidney and the other thyroid lobe were used for immunohistochemistry. After embedding in paraffin, 4 μm thick sections were stained with hematoxylin and eosin (Sigma-Aldrich) or with Masson's trichrome kit (Bio-Optica). For immunohistochemistry, sections were incubated overnight in xylene and then progressively in ethanol solution (99%-96%-70%). Endogenous

peroxidase activity was quenched with 35% H_2O_2 in methanol and target retrieval was performed in TEG buffer pH 9.2. Primary antibodies were incubated overnight at 4° C, sections were then incubated with secondary anti-rabbit HRP-conjugated antibody (Dako). Chromogenic reactions were carried out with DAB (Vector Laboratories) and stained sections were mounted with Eukitt (Bio-Optica).
For immunofluorescence analysis, thyroid sections were incubated overnight at 4°C with anti-Nis antibody (gently provided by Prof. De Felice). Sections was then incubated with secondary anti-rabbit conjugated Alexa Fluor 488; DAPI was used as nuclear counterstain. The primary antibodies used for kidney staining were: anti AQP2 and anti NKCC2 were provided by Prof. Frische; anti-Pax8, anti-Titf1 and anti-thyroglobulin were provided by Prof. De Felice; anti-cleaved Caspase-3 was purchased from Cell Signalling Technology. Zeiss Axioplan 2 microscope was used for images acquisition.
All stainings were done al least three times using different biological material sources.

Immunoblotting
Tissues were homogenized with a TissueLyser (Qiagen) in lysis buffer (300 mM sucrose; 25 mM imidazole; 1mM EDTA, 1mM PMSF) with protease and phosphatase inhibitor cocktails (Roche). Immunoblottings were performed as previously described (20). Briefly, extracted proteins were separated by SDS-PAGE, transferred onto nitrocellulose membrane and incubated with primary antibodies followed by horseradish peroxidase-conjugated secondary antibodies (Amersham Biosciences). Blots were developed using the ECL system (Amersham Biosciences). Anti NEMO, anti IKKα/β, anti p65, anti p50, anti phospho-CREB, anti CREB, anti Caspase 3 and anti β-actin antibodies were obtained from Santa Cruz Biotechnology. All immunoblots were done al least three times using different biological material sources.

RNA extraction and qPCR
1 µg of total RNA was isolated from a pool of three thyroid lobes using TRIzol Reagent (Invitrogen Life Technologies) and reverse-transcribed using Quantitec reverse transcription kit (Qiagen). qPCR reaction mixtures contained 7,5 ng of total cDNA, Power PCR Master Mix 16 (Applied Biosystems) and the following primers: Pax8, fw: GCCATGGCTGTGTAAGCAAGA, rev: GCTTGGAGCCCCCTATCACT; Titf1, fw: CTACTGCAACGGCAACCTG, rev: CCCATGCCATCATATATTCAT); Tg, fw: CATGGAATCTAATGCCAAGAACTG, rev: TCCCTGTGAGCTTTTGGAATG; Tpo, fw: CAAAGGCTGGAACCCTAATTTCT, rev: AACTTGAATGAGGTGCCTTGTCA; Nis, fw: TCCACAGGAATCATCTGCA, rev: CCACGGCCTTCATACCACC; GAPDH, forward: AATGGTGAAGGTCGGTGTG, rev: GAAGATGGTGATGGGCTTCC; c-FLIP, fw: CCGTGAAGAGACTTACAGGA, rev: GTTATGTCATGTGACTTGGG; Bcl-2, fw: GGGGTCATGTGTGTGGAGAG, rev: GCATGCTGGGGCCATATAGT; Bfl-1/A1, fw: TGCCCTGGATGTATGTGCTT, rev: GAGCATTTCCCAGATCTGTC; Bcl-xL, fw: CCTTGGATCCAGGAGAACGG, rev: AAGAGTGAGCCCAGCAGAAC;
cIAP2, fw: AGAGAGGAGCAGATGGAGCA, rev: CCTGTTCAGTGATGGCCCTT; cIAP1, fw: GACCCCTGGATAGAACACGC, rev: CTGGGGTGTCTGAAGTGGAC; Xiap, fw: GGAACATGGACATCCTCAGT, rev: TACCACTTCGCATGCTGTTC; RNA18S, fw: CGGCTACCACATCCAAGGAA, rev: GGGCCTCGAAAGAGTCCTGT. Reactions were run on a 7900HT system (Applied Biosystems). For each sample, expression of the genes of interest was normalized on the expression of RNA18S and/or GAPDH measured under the same conditions (21).

Culture of primary mouse thyrocytes
Mice of different genotypes were anesthetized and sacrificed. Thyroid lobes were dissected aseptically and placed on a microscope slide containing a drop of Eagle's minimum essential medium (EMEM). The lobes were disrupted mechanically, using two 25-gauge needles to obtain approximately ten fragments from each lobe. The fragments were transferred to a 1.5 ml tube containing 1 ml of digestion medium, consisting of 112 units/ml of type I collagenase (Sigma) and 1.2 units/ml of dispase dissolved in EMEM. The enzymatic digestion was carried out for 45 min in a 37°C water bath. The follicles were seeded and cultured in F12 medium (EuroClone) supplemented with 10% Nu-Serum IV (BD BioScience), 10 ng/ml somatostatin (Sigma Aldrich) and 2 ng/ml glycyl-L-histidyl-lysine acetate (Sigma Aldrich) in a water-saturated incubator, under air/CO_2 (95%-5%) at 37°C. TSH and TNFα used for thyrocytes stimulation were obtained from Sigma Aldrich.

Free T4 and TSH measurement
Venous blood samples were collected in

microtubes without anticoagulant. After clot formation, samples were centrifuged and the serum fraction was kept at -80°C. Free T4 was measured using the ELISA kit from DiaMetra according to the manufacturer's instructions. TSH levels were determined by rTSH (rat thyroid stimulating hormone) RIA kit (Institute of Isotopes, Budapest).

MTT assay

[3-(4,5-dimethylthiazol-2-yl)-2,5-diphenyl tetrazolium bromide] colorimetric assay for cell viability was performed in a 96-well flat-bottomed tissue culture plates as previously described (22).

Statistics

Data were analyzed by Student's t-test. A p value < 0.05 was considered significant.

RESULTS

In order to understand the role of NEMO in thyroid development and function, we applied the Cre-LoxP strategy to specifically delete the NEMO locus in the thyroid gland. For this, females bearing a floxed NEMO allele ($NEMO^{Flox/+}$), which do not show phenotype abnormalities (12), were crossed to the knock-in $Pax8^{Cre/+}$ mice, which express the Cre recombinase under the control of the endogenous Pax8 gene promoter and mediate efficient Cre recombination in thyroid (18). Mutant mice were observed at the expected mendelian frequency, and were named NEMO thyroid-specific knock-out ($NEMO^{TS\text{-}KO}$). As shown in Fig. 1A, site-specific recombination of the NEMO allele was observed only in NEMO floxed mice expressing the Cre recombinase. Efficient ablation of the NEMO locus was confirmed by immunoblot analysis on whole-thyroid extracts (Fig. 1B). Functional inactivation of the IKK complex was demonstrated by lack of I-κBα degradation in $NEMO^{TS\text{-}KO}$ thyrocytes following exposure to TNFα (Fig. 1C, left panel). On the other hand, expression of p65, IKKα/β and p50 were not affected by genetic deletion of NEMO (Fig. 1C, right panel). As $Pax8^{Cre/+}$ mice express Cre recombinase also in mesonephros and metanephros (18), excision of the NEMO floxed allele was consistently detected also in kidney tissues (Fig. 1D-E).

$NEMO^{TS\text{-}KO}$ mutant mice appeared undistinguishable from control mice at birth (data not shown). In contrast, starting from two months of age, mutant mice developed clearly smaller than control littermates and displayed a significantly reduced body weight (Fig. 2A). $NEMO^{TS\text{-}KO}$ mice had a significantly shortened life span, and about 50% of mice die before 8 months of age (Fig. 2B). When compared to control mice, $NEMO^{TS\text{-}KO}$ mice presented significantly lower levels of serum free T4 hormone (Fig. 2C), and increased thyroid stimulating hormone (TSH) levels (Fig. 2D), which is indicative of hypothyroidism. Hence, body weight reduction and early lethality observed in these mice might be due, at least in part, to thyroid dysfunction.

To exclude the possibility that the premature lethality observed in $NEMO^{TS\text{-}KO}$ mice was due to renal failure, we carried out an histological and functional analysis on the kidneys of the mutant mice. The result of this analysis, shown in Table I, indicates that partial loss of NEMO expression in specific kidney tissues was not associated with an overt kidney phenotype. In fact, monitoring of the renal function in $NEMO^{TS\text{-}KO}$ mice did not reveal any physiological alteration (Table I). Kidney histology was assessed by H/E staining and immunohistochemistry for the kidney-specific markers AQP2 and NKCC2. Again, no alteration in immunoreactivity for these markers was detected in $NEMO^{TS\text{-}KO}$ kidneys respect to control mice at 12 months of age (Figure 3A-C). From these results, we deduced that $NEMO^{TS\text{-}KO}$ do not suffer of renal dysfunction. This conclusion is consistent with a previous observation showing that podocyte-specific NEMO-deficient mice do not show overt changes in kidney morphology and functionality (17).

In order to verify whether NEMO inactivation affects thyroid embryonic development, mutant E16.5 embryos were analyzed, as Cre recombinase in $Pax8^{Cre/+}$ mice is active from E8.5 (18). At E16.5 no alteration in thyroid size and morphology could be detected (Fig. 4A), and similar results were obtained when the same analysis was performed in mice at 1 month of age (Fig. 4A). Hence, these data indicate that canonical NF-κB signaling is not required for embryonic thyroid development and differentiation.

The effect of NEMO conditional inactivation on thyroid morphology and differentiation was further analyzed. Starting from 2 months of age, thyroid glands of $NEMO^{TS\text{-}KO}$ mice appear considerably smaller compared to control mice (Fig. 4B). In the surviving 2-month-old $NEMO^{TS\text{-}KO}$ mice, significant cell loss is observed, and the thyroid follicular architecture appears highly variable in diameter with irregular outlines (Fig. 4B-F). Immunohistochemical and immunofluorescent analysis shows that

expression level of two thyroid-specific transcription factors, namely Pax8 and Ttf1, steadily declines over time (Fig. 4 CD). Similarly occurs for thyroglobulin and for the Na/I symporter Nis (Fig. 4E-F). Nis, for instance, appears barely detectable in thyrocytes isolated from two-month-old NEMO^{TS-KO} mice (Fig. 4E). Masson's trichrome staining also revealed the presence of fibrotic material in mutant thyroids (Fig. 4G). In all staining, it was clearly visible the progressive disorganization and degeneration of the thyroid parenchyma in NEMO^{TS-KO} mutant mice. Also, reduction of cellularity and gland size in NEMO^{TS-KO} mice is accompanied with massive apoptosis, as indicated by the staining for active caspase 3 (Fig. 4H).
qPCR analysis confirmed the reduced expression of the thyroid markers Pax8, Ttf1, Tpo and Nis in NEMO-deleted thyroids (Fig. 4I). The mRNA expression level of TSH receptor and thyroglobulin were also both significantly reduced (Fig. 4I). Despite its reduced expression, however, TSH receptor signaling does not appear compromised in NEMO^{TS-KO} thyrocytes, as assessed by monitoring phosphorylation of CREB following TSH stimulation (Fig. 4J).

NF-κB controls the expression of several genes, including Bfl-1/A1, Bcl-2, Bcl-xL, c-FLIP and IAPs, that protect cells against apoptotic cell death (23-29). Consistently, all these anti-apoptotic genes appear significantly down regulated in NEMO-deficient thyrocytes (Fig. 5A). Thus, we verified whether NEMO^{TS-KO} thyrocytes exhibit a greater sensitivity to apoptotic stimuli. As shown in Fig. 5 B-E, lack of NEMO dramatically sensitizes these thyrocytes to the cytotoxic action of both TNFα and TSH.

Taken together, these data demonstrate that in adult mice NEMO is required for thyrocytes survival and contributes to the maintenance of thyrocyte differentiation by regulating the expression of several thyroid markers.

DISCUSSION

In this paper, we demonstrate that NEMO signaling is essential for normal postnatal thyroid gland structure and function. Although previous studies have clearly established a role for NF-κB in thyroid tumors progression (25-27), this is the first work that examines the role of canonical NF-κB signaling in normal thyroid development and physiology. We show that mice with thyroid-specific ablation of NEMO develop a pronounced impairment of thyroid function, eventually leading to shortened life span. On the other hand, no gross alterations of thyroid gland localization, morphology and differentiation were observed during embryonic development and in newborn mice, indicating that the NEMO-dependent NF-κB signaling is not required for embryonic thyroid development. Our results indicate that in thyroid NEMO is required for at least two essential aspects, that are: i) thyrocytes survival and, ii) maintenance of thyroid markers expression. The critical role of NF-κB in cell survival is widely supported by the available literature. Gene-targeting experiments have in fact shown that mice lacking p65/RelA, IKK2, or NEMO die during embryonic development due to liver apoptosis (7-12). Thus, the extensive apoptosis observed in NEMO^{TS-KO} thyrocytes confirms the requirement for NF-κB in orchestrating cytoprotective pathways. Particularly interesting is the data showing the different behavior of wt and NEMO^{TS-KO} thyrocytes when exposed to TSH. In fact, while both wild type and NEMO^{TS-KO} thyrocytes proliferate following TSH stimulation, NEMO^{TS-KO} thyrocytes also undergo extensive apoptosis (Fig. 5). This finding is consistent with a previous evidence showing that TSH stimulation on thyrocytes in fact triggers both proliferative and apoptotic responses (33). Our work now shows that NF-κB signaling could play a decisive role in determining the fate of thyrocytes following TSH stimulation.
An interesting aspect of our experiments is the evidence here provided that NF-κB controls, directly or indirectly, the expression level of several thyroid markers. Although an involvement of NF-κB in the regulation of Nis expression has been already reported (34), we now show that, in addition to Nis, NF-κB controls the expression of a panel of thyroid markers, including Ttf1, Pax8, Tpo and thyroglobulin. In this context, our work provides a molecular explanation for some phenotypical aspects of human disorders associated with mutations in NEMO. In humans, in fact, mutations in the X-linked NEMO gene cause two distinct genetic diseases. Mutations that completely disrupt the NEMO locus result in Incontinentia Pigmenti, a disease where male patients die in utero, whereas the phenotypic analysis of females is complicated by the fact that NEMO-deficient cells quickly disappear and are replaced by wild-type cells. A second disease, named hypohydrotic ectodermal dysplasia with immune deficiency (HED-ID), is characterized by hypomorphic NEMO mutations that do not completely abolish but rather reduce NF-κB activation. HED-ID is characterized by impaired

skin appendage development and severe immune deficiency. Strikingly, hypothyroidism is not uncommon in patients with HED-ID (35-38), as predicted by the data we show here.

In conclusion, our data can be easily interpreted considering the crucial role that NEMO plays in activation of NF-κB which, in turn, regulates the expression of genes that are critical for cell survival. However, it should not be disregarded that NF-κB-independent functions have been ascribed to NEMO, and these latter are as well involved in the control of cell proliferation and cell death (39-41). Hence, it is well possible that NF-κB-independent functions of NEMO may contribute, at least in part, to the cellular degeneration observed in $NEMO^{TS-KO}$ thyrocytes.

ACKNOWLEDGMENTS

We thank Drs. Antonella Fierro and Marianna Scrima for technical assistance; Prof. Mario De Felice for critical reading of the manuscript.

Conflict of interest statement: None of the authors has a conflict of interest with the submitted material.

Author contributions:
CR, AI, AF, LEDA, PM, IS, RL, TZ, and TC performed the experiments and analyzed data; AL, MZ, GC, MP, MS, PV and RS conceived experiments and analyzed data; PV wrote the manuscript.

REFERENCES

1. Vallabhapurapu, S., Karin, M. (2009) Regulation and function of NF-kappaB transcription factors in the immune system. *Annu. Rev. Immunol.* **27,** 693-733

2. Sebban, H., Yamaoka, S., Courtois, G. (2006) Posttranslational modifications of NEMO and its partners in NF-kappaB signaling. *Trends Cell Biol.* **16,** 569-77.

3. Shifera, A. S. (2010) Protein-protein interactions involving IKKgamma (NEMO) that promote the activation of NF-kappaB. *J. Cell Physiol.* **223,** 558-561.

4. Chen, Z. J. (2012) Ubiquitination in signaling to and activation of IKK. *Immunol. Rev.* **246,** 95-106.

5. Zotti, T., Scudiero, I., Settembre, P., Ferravante, A., Mazzone, P., D'Andrea, L., Reale, C., Vito, P., Stilo, R. (2014) TRAF6-mediated ubiquitination of NEMO requires p62/sequestosome-1. *Mol. Immunol.* **58,** 27-31.

6. Zotti, T., Uva, A., Ferravante, A., Vessichelli, M., Scudiero, I., Ceccarelli, M., Vito, P., Stilo, R. (2011) TRAF7 protein promotes Lys-29-linked polyubiquitination of IkappaB kinase (IKKgamma)/NF-kappaB essential modulator (NEMO) and p65/RelA protein and represses NF-kappaB activation. *J. Biol. Chem.* **286,** 22924-22933.

7. Beg, A., Sha, C., Bronson, T., Ghosh, S., and Baltimore, D. (1995) Embryonic lethality and liver degeneration in mice lacking the RelA component of NF-kB. *Nature* **376**, 167-170.

8. Li, Q., Van Antwerp, D., Mercurio, F., Lee, K. F., and Verma, I. M. (1999) Severe liver degeneration in mice lacking the IkB kinase 2 gene. *Science* **284**, 321-325.

9. Li, Z. W., Chu, W., Hu, Y., Delhase, M., Deerinck, T., Ellisman, M., Johnson, R., and Karin. M. (1999) The IKKb subunit of IkB kinase (IKK) is essential for nuclear factor kB activation and prevention of apoptosis. *J. Exp. Med.* **189,** 1839-1845.

10. Tanaka, M., Fuentes, M. E., Yamaguchi, K., Durnin, M. H., Dalrymple, S. A., Hardy, K. L., and Goeddel, D. V. (1999) Embryonic lethality, liver degeneration, and impaired NF-kB activation in IKK-b-deficient mice. *Immunity* **10**, 421-429.

11. Rudolph, D., Yeh, C., Wakeham, A., Rudolph, B., Nallainathan, D., Potter, J., Elia, A. J., and Mak, T. W. (2000) Severe liver degeneration and lack of NF-kB activation in NEMO/IKKgamma deficient mice. *Genes Dev.* **14,** 854–862.

12. Schmidt-Supprian, M., Bloch, W., Courtois, G., Addicks, K., Israël, A., Rajewsky, K., and Pasparakis, M. (2000) NEMO/IKKg-deficient mice model incontinentia pigmenti. *Mol Cell* **5**, 981–992.

13. Luedde, T., Beraza, N., Kotsikoris, V., van Loo, G., Nenci, A., De Vos, R., Roskams, T., Trautwein, C., and Pasparakis, M. (2007) Deletion of NEMO/IKKgamma in liver parenchymal cells causes steatohepatitis and hepatocellular carcinoma. *Cancer Cell* **11**, 119-132.

14. Nenci, A., Becker, C., Wullaert, A., Gareus, R., van Loo, G., Danese, S., Huth, M., Nikolaev, A., Neufert, C., Madison, B., Gumucio, D., Neurath, M. F., and Pasparakis, M. (2007) Epithelial NEMO links innate immunity to chronic intestinal inflammation. *Nature* **446**, 557-561.

15. van Loo, G., De Lorenzi, R., Schmidt, H., Huth, M., Mildner, A., Schmidt-Supprian, M., Lassmann, H., Prinz, M. R., and Pasparakis, M. (2006) Inhibition of transcription factor NF-kappaB in the central nervous system ameliorates autoimmune encephalomyelitis in mice. *Nat. Immunol.* **7,** 954-961.

16. Kratsios, P., Huth, M., Temmerman, L., Salimova, E., Al Banchaabouchi, M., Sgoifo, A., Manghi, M., Suzuki, K., Rosenthal, N., and Mourkioti F. (2010) Antioxidant amelioration of dilated cardiomyopathy caused by conditional deletion of NEMO/IKKgamma in cardiomyocytes. *Circ. Res.* **106,** 133-144.

17. Brähler, S., Ising, C., Hagmann, H., Rasmus, M., Hoehne, M., Kurschat, C., Kisner, T., Goebel, H., Shankland, S., Addicks, K., Thaiss, F., Schermer, B., Pasparakis, M., Benzing, T., and Brinkkoetter, P. T. (2012) Intrinsic proinflammatory signaling in podocytes contributes to podocyte damage and prolonged proteinuria. *Am. J. Physiol. Renal. Physiol.* **303,** F1473-85.

18. Bouchard, M., Souabni, A., and Busslinger, M. (2004) Tissue-specific expression of Cre recombinase from the Pax8 locus. *Genesis* **38,** 105-109.

19. Iervolino, A., Trepiccione. F., Petrillo, F., Spagnuolo, M., Scarfò, M., Frezzetti, D., De Vita, G., De Felice, M., and Capasso, G. (2015). Selective dicer suppression in the kidney alters GSK3β/β-catenin pathways promoting a glomerulocystic disease. *PLoS One* **10,** e0119142.

20. Stilo, R., Liguoro, D., di Jeso, B., Leonardi, A., and Vito, P. (2003) The alpha-chain of the nascent polypeptide- associated complex binds to and regulates FADD function. *Biochem. Biophys. Res. Commun.* **303,** 1034-1041.

21. D'Andrea, E.L., Ferravante, A., Scudiero, I., Zotti, T., Reale, C., Pizzulo, M., De La Motte, L. R., De Maio, C., Mazzone, P., Telesio, G., Vito, P., and Stilo, R. (2014) The Dishevelled, EGL-10 and pleckstrin (DEP) domain-containing protein DEPDC7 binds to CARMA2 and CARMA3 proteins, and regulates NF-κB activation. *PLoS One* **9,** e116062.

22. Scudiero, I., Zotti, T., Ferravante, A., Vessichelli, M., Vito, P., and Stilo, R. (2011) Alternative splicing of CARMA2/CARD14 transcripts generates protein variants with differential effect on NF-κB activation and endoplasmic reticulum stress-induced cell death. *J. Cell Physiol.* **226**, 3121-3131.

23. Zong, W., X., Edelstein, L., C., Chen, C., Bash, J., and Gélinas, C. (1999) The prosurvival Bcl-2 homolog Bfl-1/A1 is a direct transcriptional target of NF-kappaB that blocks TNFalpha-induced apoptosis. *Genes Dev.* **13,** 382-387.

24. Micheau, O., Lens, S., Gaide, O., Alevizopoulos, K., and Tschopp J. (2001) NF-kappaB signals induce the expression of c-FLIP. *Mol. Cell. Biol.* **21,** 5299-5305.

25. Chu, Z., L., McKinsey, T., A., Liu, L., Gentry, J. J., Malim, M., H., and Ballard D.,W. (1997) Suppression of tumor necrosis factor-induced cell death by inhibitor of apoptosis c-IAP2 is under NF-kappaB control. *Proc. Natl. Acad. Sci. U S A* **94,** 10057-10062.

26. Wang, C., Y., Mayo, M. W., Korneluk, R. G., Goeddel, D. V., and Baldwin, A. S. Jr. (1996) NF-kappaB antiapoptosis: induction of TRAF1 and TRAF2 and c-IAP1 and c-IAP2 to suppress caspase-8 activation. *Science* **281,** 1680-1683.

27. Stehlik, C., de Martin, R., Kumabashiri, I., Schmid, J., A., Binder, B., R., and Lipp, J. (1998) Nuclear factor (NF)-kappaB-regulated X-chromosome-linked iap gene expression protects endothelial cells from tumor necrosis factor alpha-induced apoptosis. *J. Exp. Med.* **188,** 211-216.

28. Khoshnan, A., Tindell, C., Laux, I., Bae, D., Bennett, B., and Nel, A. E. (2000) The NF-kappa B cascade is important in Bcl-xL expression and for the anti-apoptotic effects of the CD28 receptor in primary human CD4+ lymphocytes. *J. Immunol.* **165,** 1743-1754.

29. Guiet, C., Silvestri, E., De Smaele, E., Franzoso, G., and Vito, P. (2002) c-FLIP efficiently rescues TRAF-2$^{-/-}$ cells from TNF- induced apoptosis. *Cell Death Differ.* **9,** 138-144.

30. Visconti, R., Cerutti, J., Battista, S., Fedele, M., Trapasso, F., Zeki, K., Miano, M. P., de Nigris, F., Casalino, L., Curcio, F., Santoro, M., and Fusco, A. (1997) Expression of the neoplastic phenotype by human thyroid carcinoma cell lines requires NFkappaB p65 protein expression. *Oncogene* **15,** 1987-1994.

31. Pacifico, F., Mauro, C., Barone, C., Crescenzi, E., Mellone, S., Monaco, M., Chiappetta, G., Terrazzano, G., Liguoro, D., Vito, P., Consiglio, E., Formisano, S., and Leonardi A. (2004) Oncogenic and anti-apoptotic activity of NF-kappa B in human thyroid carcinomas. *J. Biol. Chem.* **279**, 54610-54619.

32. Pacifico, F., and Leonardi, A. (2010) Role of NF-kappaB in thyroid cancer. *Mol. Cell. Endocrinol.* **321,** 29-35.

33. De Gregorio, G., Coppa, A., Cosentino, C., Ucci, S., Messina, S., Nicolussi, A., D' Inzeo, S., Di Pardo, A., Avvedimento, E. V., and Porcellini A. (2007) The p85 regulatory subunit of PI3K mediates TSH-cAMP-PKA growth and survival signals. *Oncogene* **26,** 2039-2047.

34. Nicola, P., Nazar, M., Mascanfroni, D., Pellizas, C. G., and Masini-Repiso, A. M. (2010) NF-kappaB p65 subunit mediates lipopolysaccharide- induced Na+/I- symporter gene expression by involving functional interaction with the paired domain transcription factor Pax8. *Mol. Endocrinol.* **24,** 1846-1862.

35. Fryns, P., Chrzanowska, K., and Van den Berghe, H. (1989) Hypohidrotic ectodermal dysplasia, primary hypothyroidism, and agenesis of the corpus callosum. *J. Med. Genet.* **26,** 520-521.

36. Pike, G., Baraitser, M., Dinwiddie, R., and Atherton, D. J. (1986) A distinctive type of hypohidrotic ectodermal dysplasia featuring hypothyroidism. *J. Pediatr.* **108,** 109-111.

37. Pabst, F., Groth, O., and McCoy, E. (1981) Hypohidrotic ectodermal dysplasia with hypothyroidism. *J. Pediatr.* **98,** 223-227.

38. Sundaravalli, A., and Shetty, V. (1980) Congenital hypothyroidism with ectodermal dysplasia. *Indian Pediatr.* **17,** 566.

39. Bettermann, K., Vucur, M., Haybaeck, J., Koppe, C., Janssen, J., Heymann, F., Weber, A., Weiskirchen, R., Liedtke, C., Gassler, N., Müller, M., de Vos, R., Wolf, M.J., Boege, Y., Seleznik, G.M., Zeller, N., Erny, D., Fuchs, T., Zoller, S., Cairo, S., Buendia, M.A., Prinz, M., Akira, S., Tacke, F., Heikenwalder, M., Trautwein, C. and Luedde, T. (2010) TAK1 suppresses a NEMO-dependent but NF-kappaB-independent pathway to liver cancer. *Cancer Cell* **17**, 481-496.

40. Legarda-Addison, D., Hase, H., O'Donnell, M.A. and Ting, A.T. (2009) NEMO/IKKgamma regulates an early NF-kappaB-independent cell-death checkpoint during TNF signaling. *Cell Death Differ.* **16,** 1279-1288.

41. Comb, W.C., Hutti, J.E., Cogswell, P., Cantley, L.C. and Baldwin, A.S. (2012) p85α SH2 domain phosphorylation by IKK promotes feedback inhibition of PI3K and Akt in response to cellular starvation. *Mol. Cell* **45**, 719-730.

FIGURE LEGENDS

Table I Renal physiology parameters in NEMO^{TS-KO} mice.

Figure 1 Generation of thyroid-specific NEMO knockout mice. A) PCR analysis of thyroid genomic DNA extracted from one-month-old mice of the indicated genotypes. For amplification of NEMO alleles, two different primer sets were used, one amplifying the floxed region, and the other amplifying the allele resulting from excision (12). Pax8-Cre allele were amplified with a primer set enabling to distinguish the Cre-encoding allele from the wild-type allele. B) Thyroid extracts from 8-week-old NEMO^{TS-KO} mice and littermate control mice were analyzed by immunoblot assay. Actin blot served as loading control. C) Protein extracts prepared from NEMO^{TS-KO} and wild-type cultured thyrocytes at the indicated time points after TNFα stimulation (10ng/ml) were assessed for I-κBα degradation (*left panel*) and expression of components of the NF-κB pathway (*right panel*) by immunoblot analysis. D-E) Genomic and immunoblot analysis in the kidney cortex, inner stripe of the outer medulla (ISOM) and inner medulla (IM) of NEMO^{TS-KO} and control mice.

Figure 2 Early lethality of NEMO^{TS-KO} mice A) Body weight of male NEMO^{TS-KO} and control mice at one month after birth (n = 12 for each genotype). p value was calculated with Student's t-test comparing both groups. B) Survival rates of NEMO^{TS-KO} and control mice (n = 10 for each) during 12 months after birth. C) ELISA assay of free T4 serum level in NEMO^{TS-KO} and control mice (n = 10 for each group) at the indicated months after birth. D) TSH serum level in NEMO^{TS-KO} and control mice at 12 months after birth (n = 7 for each group).

Figure 3 NEMO^{TS-KO} mice kidney phenotype analysis. A) Hematoxylin and eosin (H&E) staining and B) immunohistochemical analysis of the kidney markers NKCC2 and AQP2 in control and NEMO^{TS-KO} kidney sections at 12 months of age (OM, outer medulla; IM, inner medulla). C) Quantification of AQP2 positive cells in the collecting ducts (CD) of the inner medulla. Count was carried out on images acquired from 5 NEMO^{TS-KO} and 5 control mice. Data shown is representative of at least three independent experiments.

Figure 4 Down-regulation of thyroid markers and apoptosis in NEMO^{TS-KO} thyroid. Hematoxylin and eosin staining (A, B) and immunohistochemical analysis of C) Pax8, D) Ttf1, F) thyroglobulin and H) active caspase 3 in control and NEMO^{TS-KO} thyroid sections at the indicated age. G) Masson's trichromic staining in NEMO^{TS-KO} and control thyroids. Fibrotic material appears as a blue staining (black arrows). E) Immunofluorescence analysis of Nis in NEMO^{TS-KO} and control mice. I) *Left panel* Quantitative PCR expression analysis of the indicated genes in thyroids isolated from NEMO^{TS-KO} and control mice at 12 months of age. Each RNA sample was obtained by pooling three thyroids/genotype. Data shown (mean + SEM, n = 3) is representative of at least three independent experiments done in triplicate. *Right panel* Immunoblot analysis of thyroid markers in thyrocytes isolated from NEMO^{TS-KO} and control mice. J) Western blot analyses of total and phosphorylated CREB in protein extracts from NEMO^{TS-KO} and control thyrocytes left untreated or stimulated with TSH (1 mU/ml) for 30 min.

Figure 5 Increased sensitivity of NEMO^{TS-KO} thyrocytes to apoptosis. A) Quantitative PCR expression analysis of the indicated anti-apoptotic genes in thyrocytes isolated from 12-month-old NEMO^{TS-KO} and control mice left untreated or stimulated with TNFα (10ng/ml) for 7 hrs. Each RNA sample was obtained by pooling three thyroids/genotype. Data shown (mean + SEM, n = 3) is representative of at least three independent experiments done in triplicate. B) Thyrocytes from six-month-old NEMO^{TS-KO} and wild type mice were left untreated or treated with TNFα (10ng/ml) or TSH (1 mU/ml) for 24 hrs, and cell viability was measured by MTT assay. Data shown (mean + SEM, n = 3) is representative of at least three independent experiments done in triplicate. C) Phase-contrast micrographs of thyreocytes treated as in B). D) Immunoblot assay of caspase 3 from proteic lysates of thyreocytes treated as in B). Activation of caspase 3 can be inferred from processing of the p32 precursor. E) Immunoblot assay (*left panel*) and its densitomentric analysis (*right panel*) of NEMO expression in purified thyrocytes used for the experiments shown above. Data shown is representative of at least three independent experiments.

TABLE I

12-month-old mice		NEMO^{TS-KO}	n.	CTR	n	p val. NEMO^{TS-KO} vs. CTR
Weight	gr	26.25 ± 0.77	14	30.02 ± 1.06	11	0.0037
Urine Output	µl/min/gbw	52.74 ± 4.31	11	46.05 ± 4.50	9	0.454
Proteinuria	mg/24hrs	2.1 ± 0.25	11	1.94 ± 0.22	9	0.65
Urinary pH	pH	7.03 ± 0.39	7	7.06 ± 0.40	7	0.95
Na/Creatinine	mM/mM	36.8 ± 2.76	10	32.28 ± 2.24	9	0.23
K/Creatinine	mM/mM	49 ± 3.82	10	37.59 ± 4.63	9	0.07
Cl/Creatinine	mM/mM	74 ± 3.63	10	73.36 ± 3.48	9	0.89

Fig. 1

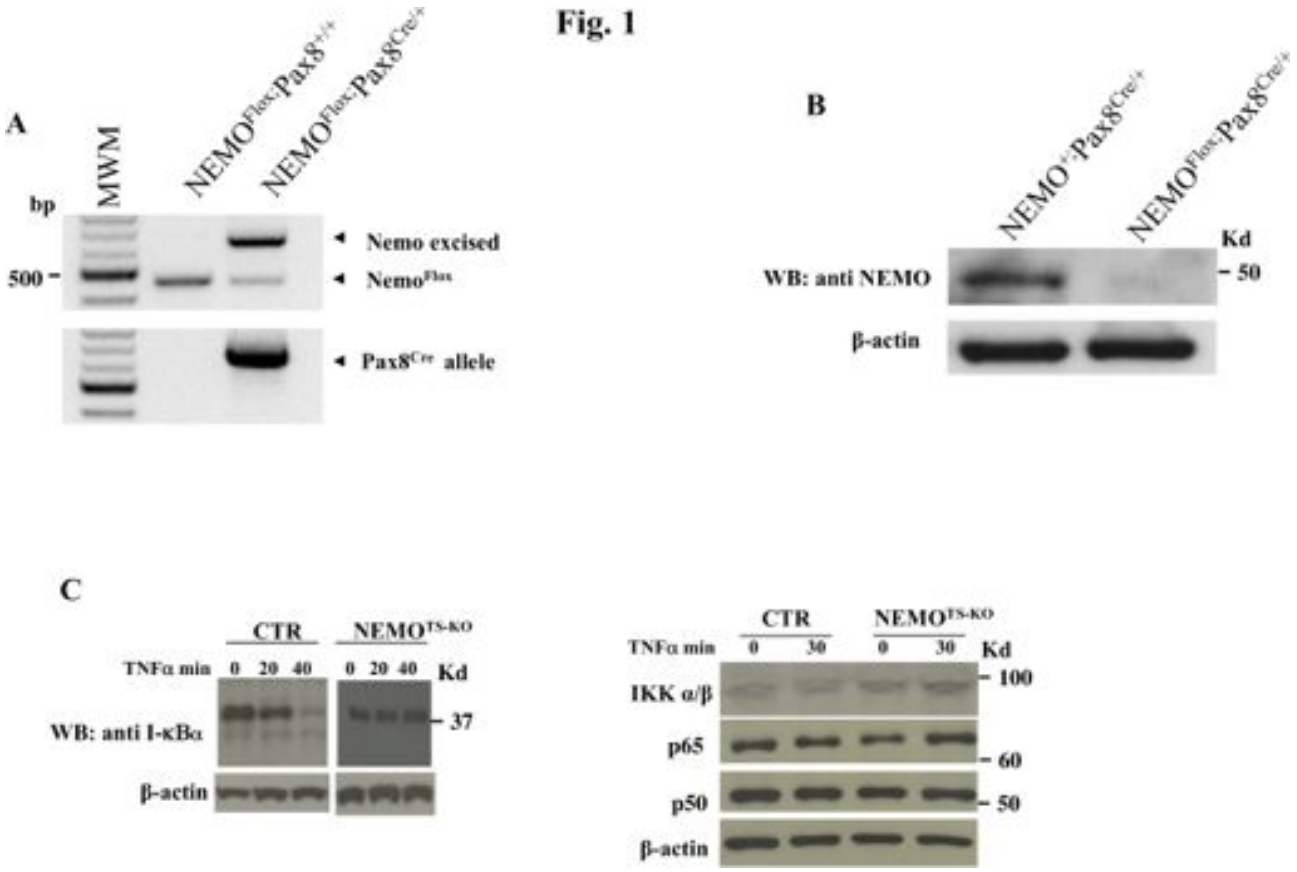

Fig. 1

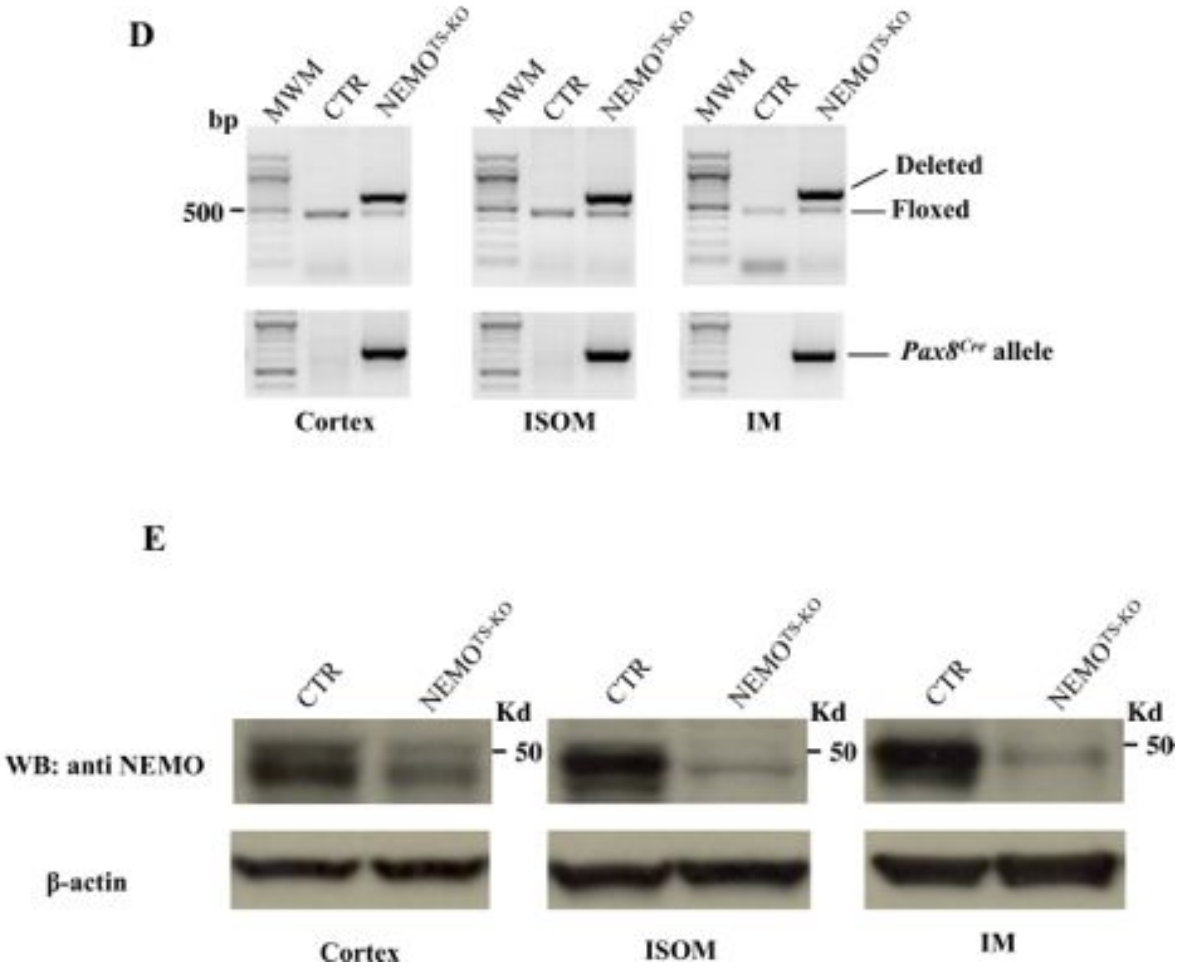

Fig. 2

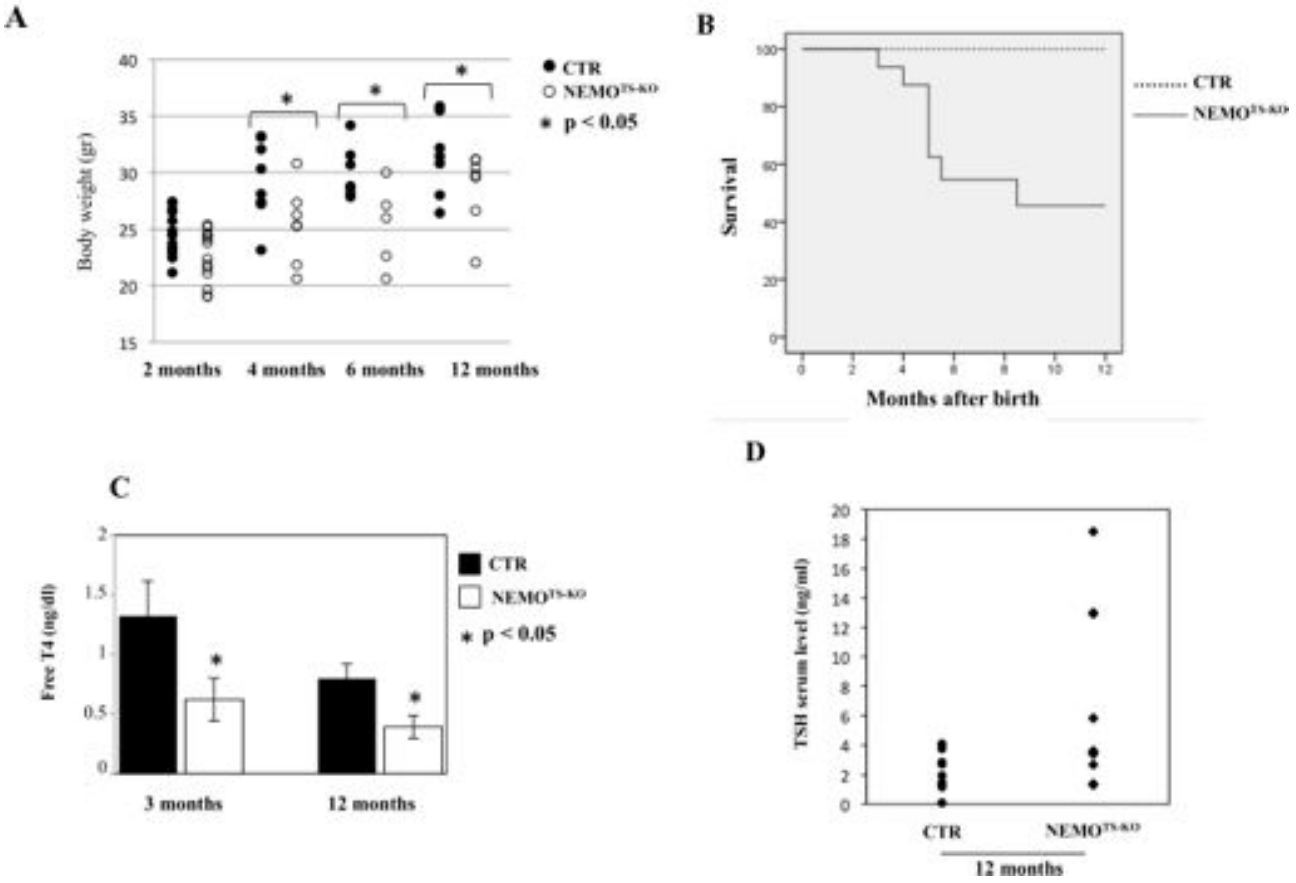

Fig. 3

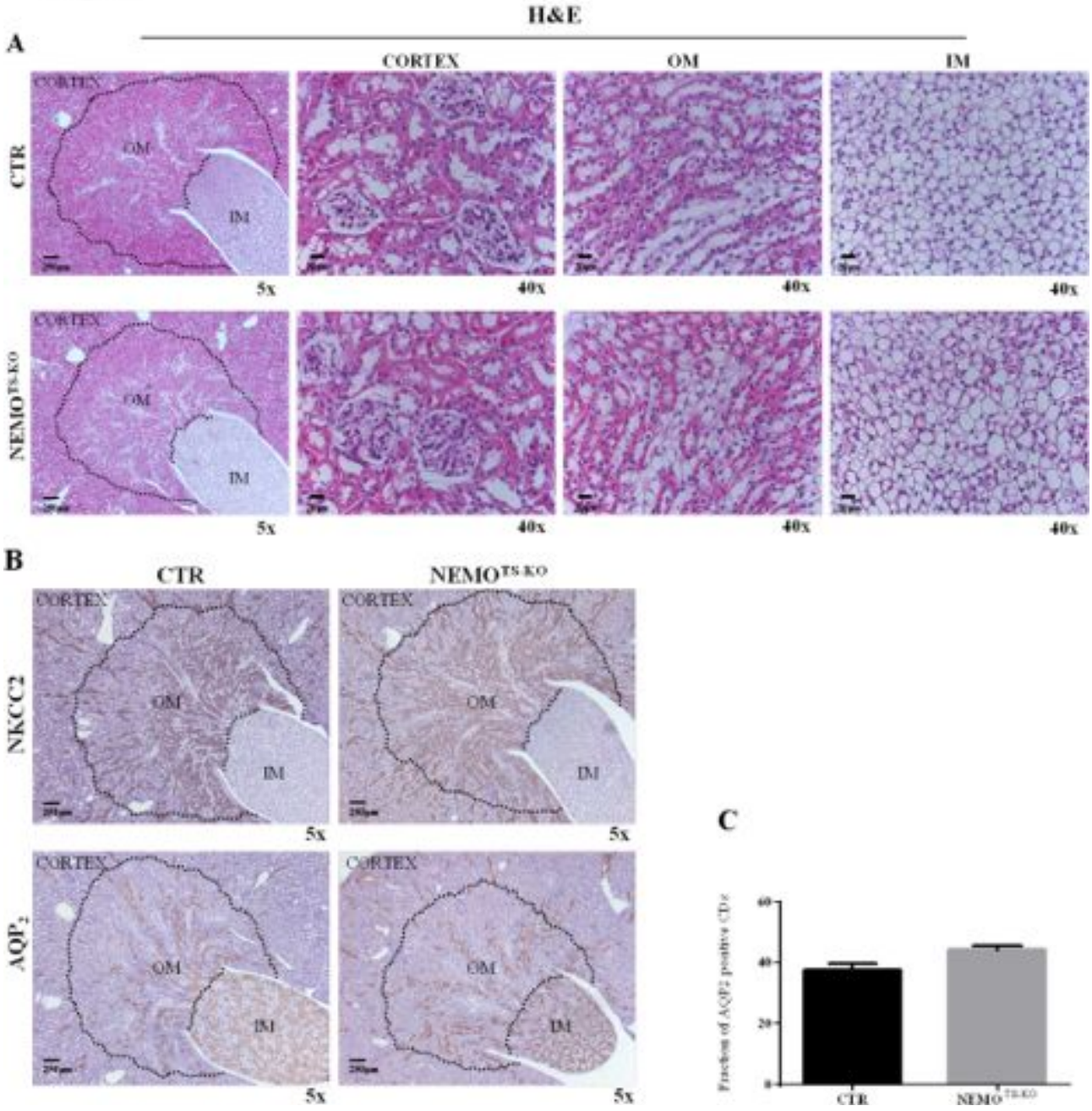

Fig. 4

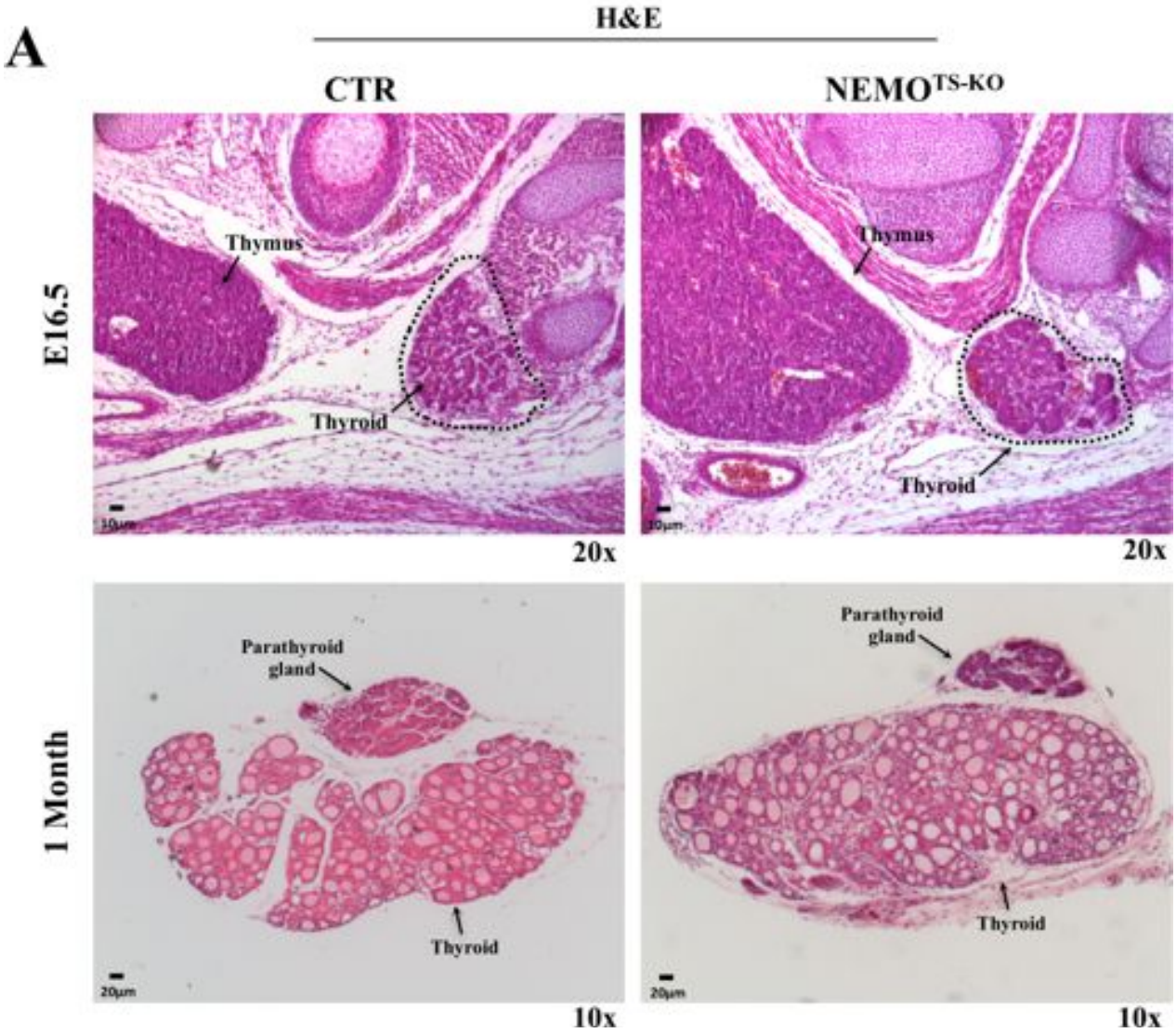

Fig. 4

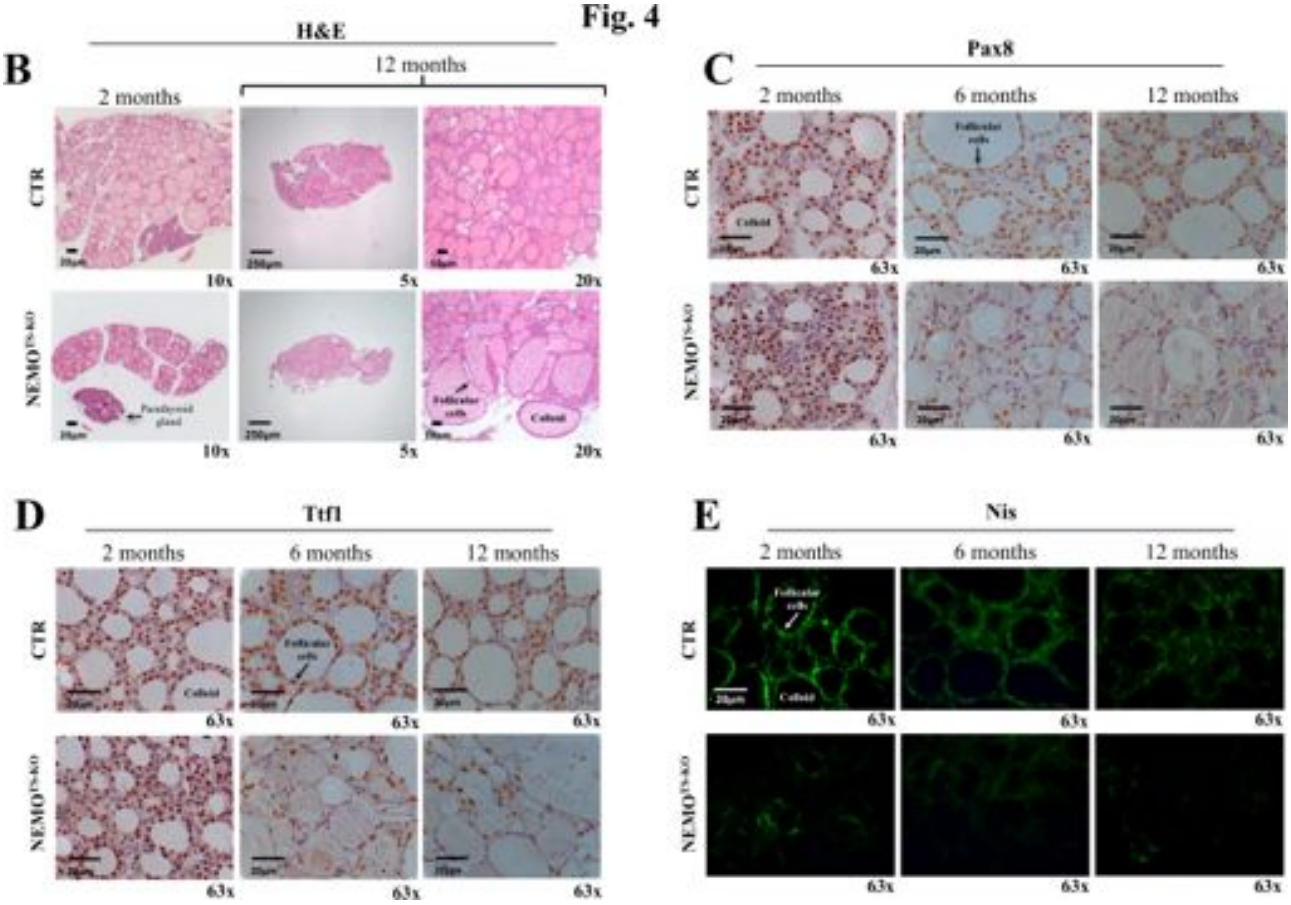

Fig. 4

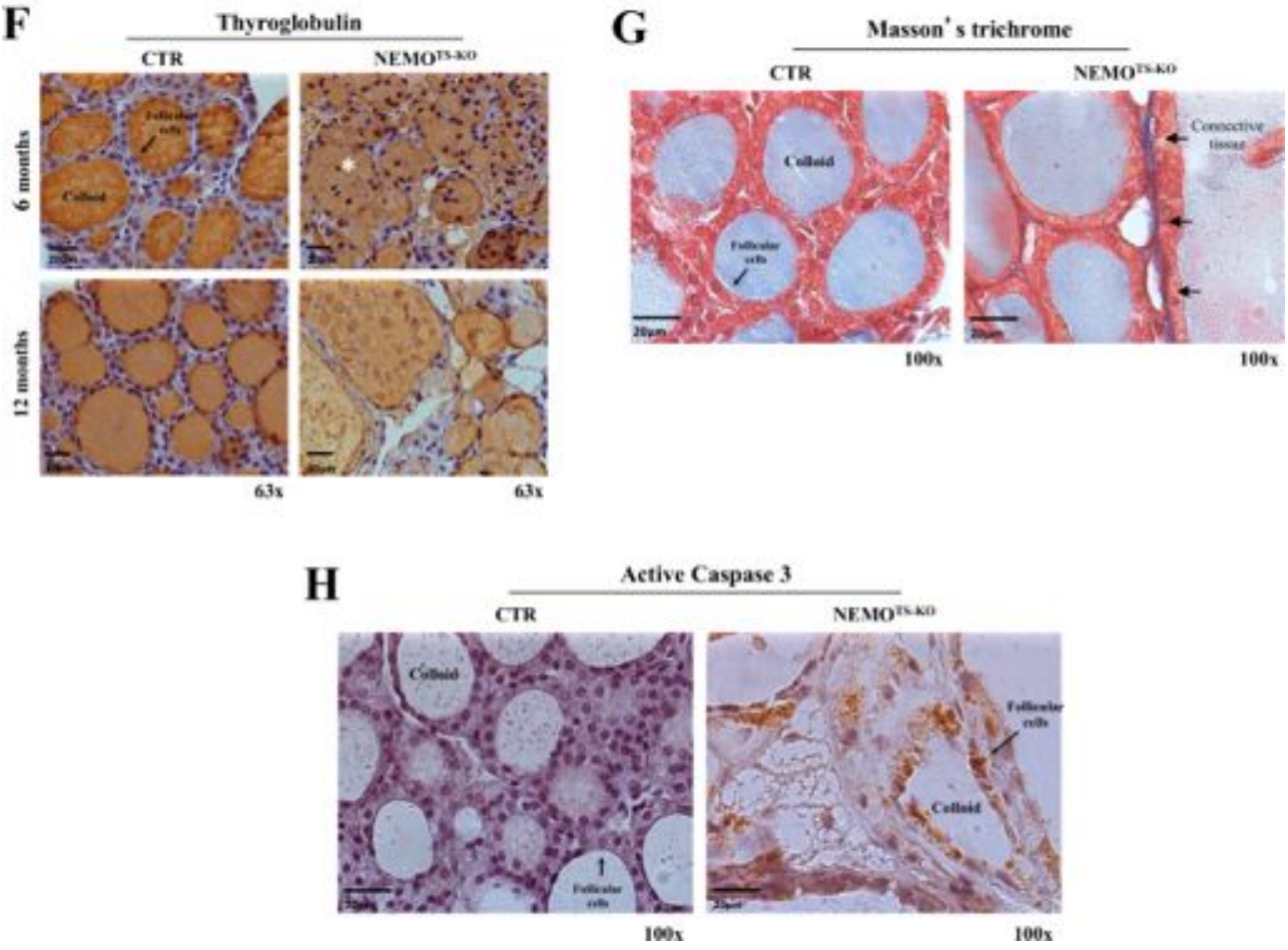

Fig. 4

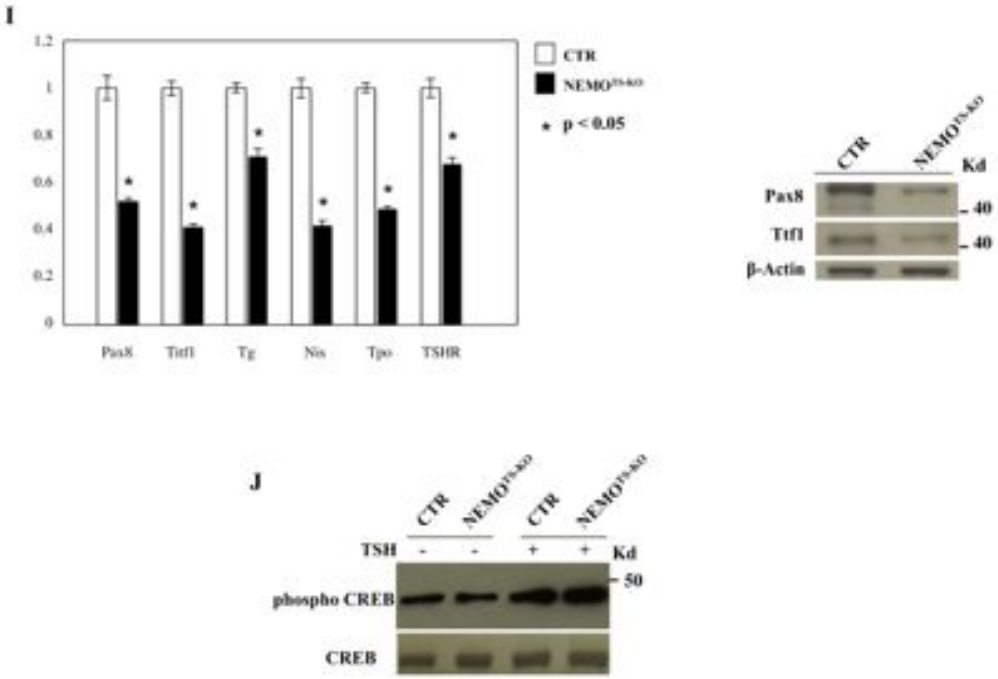

Fig. 5

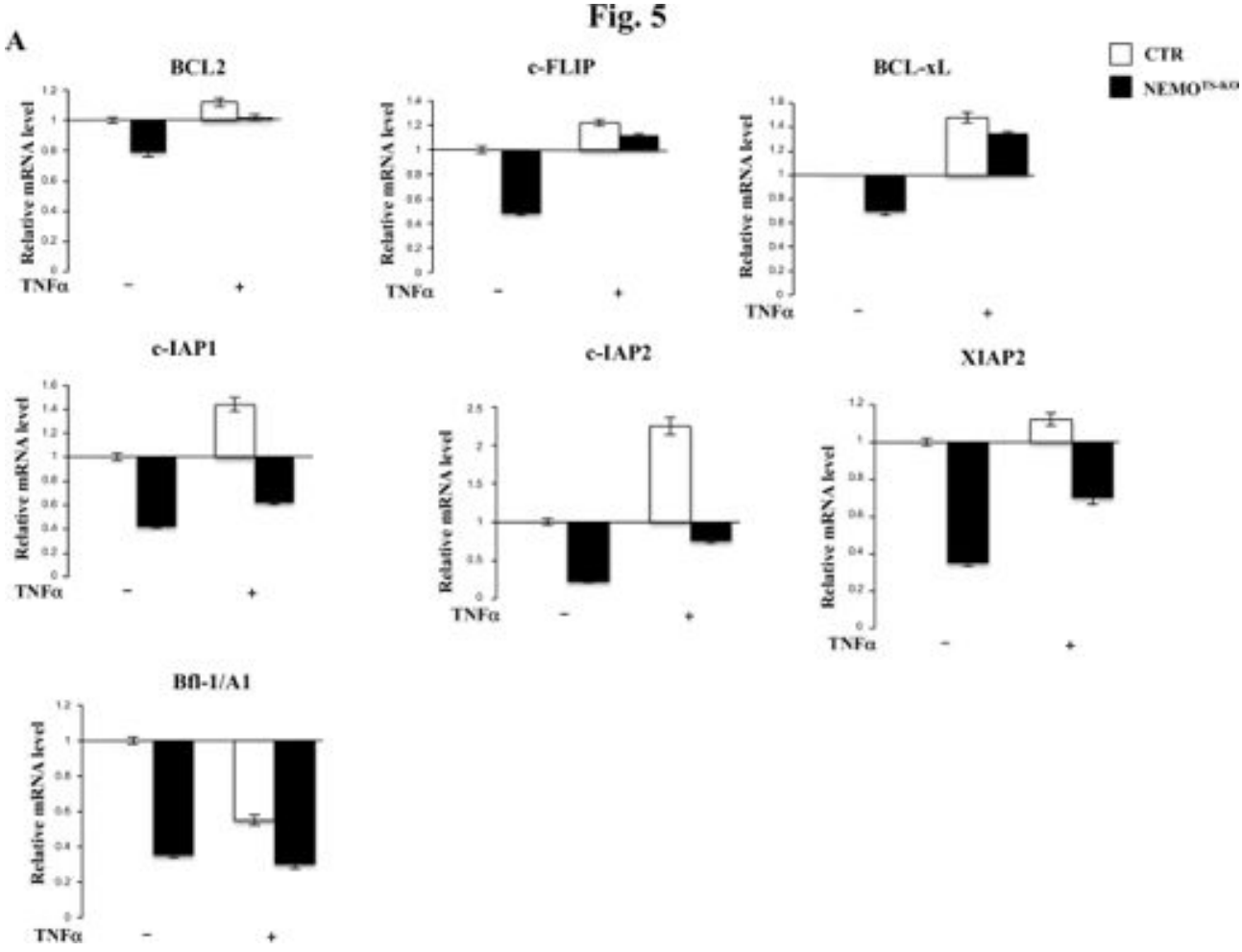

Fig. 5

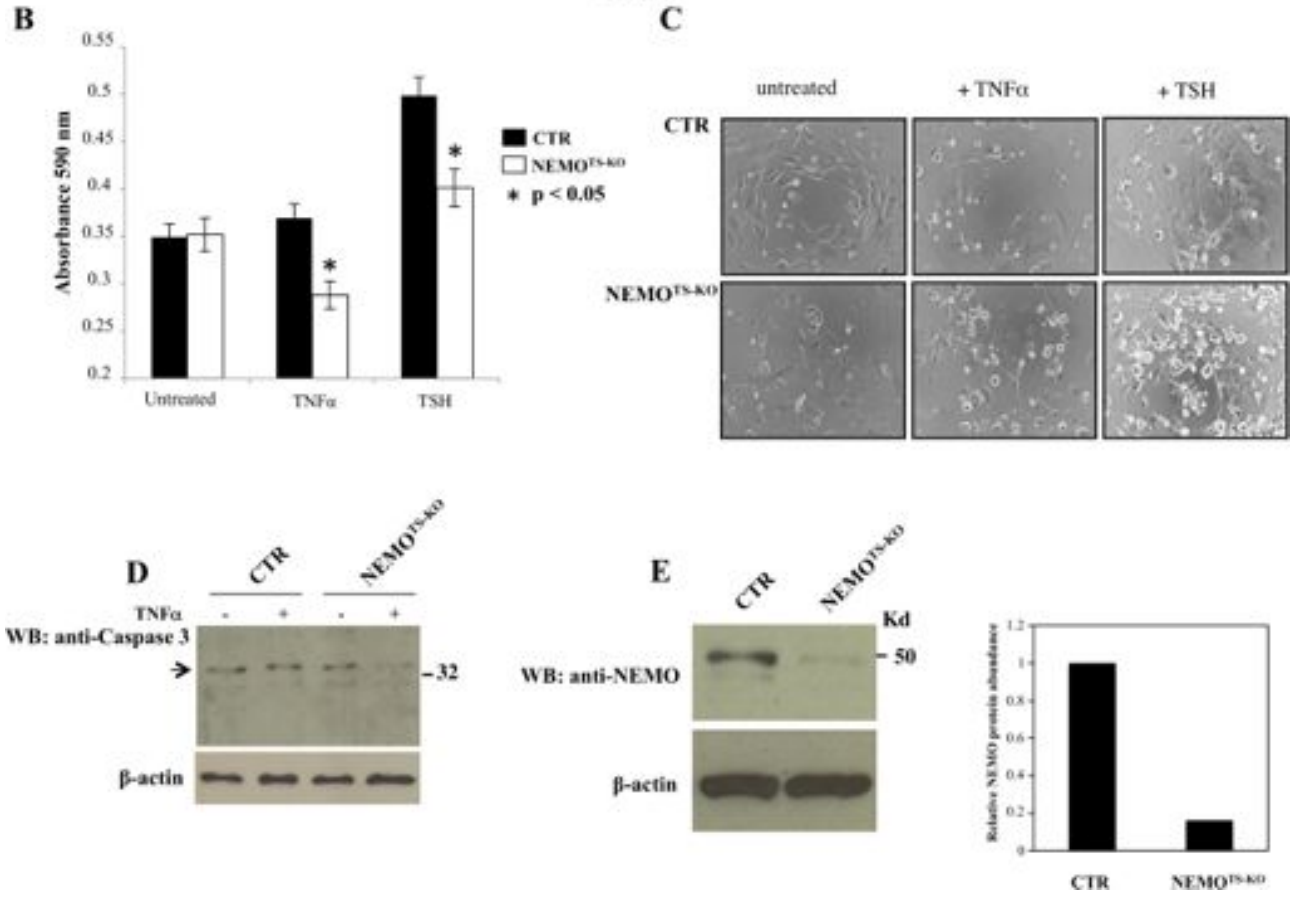

NF-kB Essential MOdulator (NEMO) Is Critical for Thyroid Function

Carla Reale, Anna Iervolino, Ivan Scudiero, Angela Ferravante, Luca Egildo D'Andrea, Pellegrino Mazzone, Tiziana Zotti, Antonio Leonardi, Luca Roberto, Mariastella Zannini, Tiziana De Cristofaro, Muralitharan Shanmugakonar, Giovambattista Capasso, Manolis Pasparakis, Pasquale Vito and Romania Stilo

J. Biol. Chem. published online January 19, 2016
